Journal of Alloys and Compounds 511 (2012) 237–241

Contents lists available at SciVerse ScienceDirect

Journal of Alloys and Compounds

journal homepage: www.elsevier.com/locate/jallcom

Strain enhancement in $Bi_{1/2}(Na_{0.82}K_{0.18})_{1/2}TiO_3$ lead-free electromechanical ceramics by co-doping with Li and Ta

Van-Quyet Nguyen[a], Hyoung-Su Han[a], Kyung-Jong Kim[a], Duc-Dung Dang[b], Kyoung-Kwan Ahn[c], Jae-Shin Lee[a,*]

[a] School of Materials Science and Engineering, University of Ulsan, Ulsan, Republic of Korea
[b] Department of Physics, University of Ulsan, Ulsan, Republic of Korea
[c] School of Mechanical Engineering, University of Ulsan, Ulsan, Republic of Korea

ARTICLE INFO

Article history:
Received 8 July 2011
Received in revised form
14 September 2011
Accepted 15 September 2011
Available online 19 September 2011

Keywords:
Ferroelectrics
Sintering
Piezoelectricity
Electrostriction
Strain

ABSTRACT

The effects of co-doping with Ta- and Li-ions on the microstructure, crystal structure, ferroelectric, and electric field-induced strain properties of $Bi_{1/2}(Na_{0.82}K_{0.18})_{1/2}TiO_3$ (BNKT) ceramics were investigated. Li substitution into Na-sites led to a ferroelectric-nonpolar phase transition and a large accompanying normalized strain (S_{max}/E_{max}) of 727 pm/V near the phase boundary, when 2.5 mol% Li and 2.5 mol% Ta were co-doped on A- and B-sites, respectively. The phase transition-related strain was thought to be induced by a decrease in the tolerance factor of the perovskite structure.

1. Introduction

Recently, lead-free bismuth perovskite ceramics have attracted attention as possible alternatives for Pb-containing lead zirconate titanate (PZT) that have primarily been used as piezoelectric sensors and electromechanical actuators [1–4].

Orthorhombic bismuth sodium titanate, $(Bi_{1/2}Na_{1/2})TiO_3$ (BNT), is thought to be an excellent lead-free piezoelectric ceramic candidate because of its large remnant polarization (P_r = 38 μC/cm^2) and high Curie temperature (T_c = 320 °C) [5]. However, its high conductivity and high coercive field (E_c = 73 kV/cm) can cause problems in the poling process, and thus limit its practical applications [5–8]. Such a barrier was found to be overcome by forming solid solutions with tetragonal perovskites such as $BaTiO_3$ (BT) [1–3,9,10] or $(Bi_{1/2}K_{1/2})TiO_3$ (BKT) [11–15]. Moreover, a giant electric field-induced strain (EFIS) comparable to that in soft PZT counterparts has been reported for BNT–$BaTiO_3$–(K,Na)NbO_3 (BNT–BT–KNN) ceramics [16,17]. This system recently showed strong relaxations in terms of frequency dependence of the dielectric properties near phase transition temperatures [10].

On the other hand BNT–BKT (BNKT) solid solutions exhibit higher piezoelectric properties near the morphotropic phase boundary, where the BKT concentration ranges from 16% to 20% [11–15]. More recently, it was found that large strains in BNKT (Na/K = 82/18 or 78/22) ceramics can be observed when B-site Ti ions are substituted with either isovalent ions such as Hf [18] and Zr [19] or aliovalent ions including Nb [20] and Ta [21]. In light of this observation, it is useful to examine the effect of simultaneous A- and B-site substitution on EFIS in BNKT. This work investigates the EFIS of BNKT ceramics co-doped with Li and Ta at the A- and B-sites, respectively, with a series of compositions in the $(Bi_{0.5}Na_{0.41-x}K_{0.09}Li_x)(Ti_{1-y}Ta_y)O_3$ system. Since Ta-substituted BNKT was reported to reveal large strains when the Ta concentration lies in the range of 2–3 mol% [21], this work fixes the Ta doping level y at 0.025, while Li content x is varied in the range of 0–0.1.

2. Experimental

A conventional solid state reaction route was applied to prepare powders with compositions of $(Bi_{0.5}Na_{0.41-x}K_{0.09}Li_x)(Ti_{1-y}Ta_y)O_3$, where $\{x, y\} = \{(0, 0), (0, 0.025), (0.025, 0.025), (0.050, 0.025), (0.075, 0.025), \text{and } (0.100, 0.025)\}$. Powders of Bi_2O_3, K_2CO_3, Ta_2O_5, TiO_2, Li_2CO_3 (99.9%, Kojundo Chemical, Japan) and Na_2CO_3 (99.9%, Ceramic Specialty Inorganics) were used as raw materials. First, the powders were weighed according to chemical formula and then ball-milled for 24 h in anhydrous ethanol with zirconia balls. The slurry was dried and calcined at 850 °C for 2 h. The calcined powder was pressed at 200 MPa into circular pellets with a diameter of

* Corresponding author. Tel.: +82 52 259 2286; fax: +82 52 259 1688.
E-mail address: jslee@ulsan.ac.kr (J.-S. Lee).

0925-8388/$ – see front matter © 2011 Elsevier B.V. All rights reserved.
doi:10.1016/j.jallcom.2011.09.043

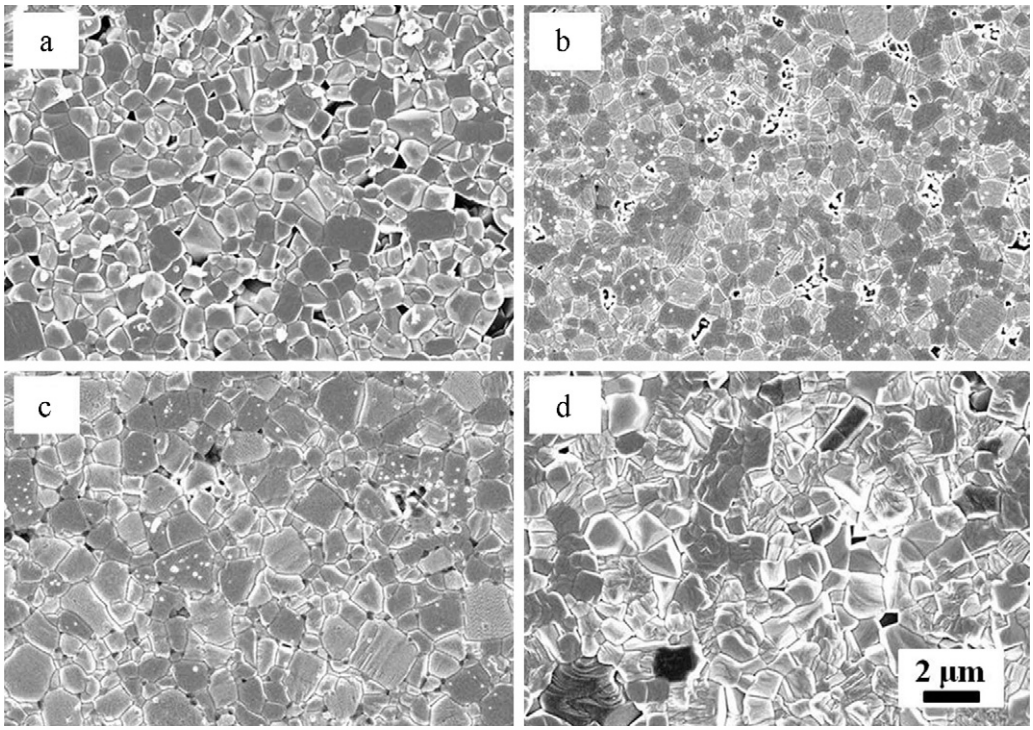

Fig. 1. Polished and thermally etched surface micrographs of $(Bi_{0.5}Na_{0.41-x}K_{0.09}Li_x)(Ti_{1-y}Ta_y)O_3$ ceramics sintered at 1150 °C for 2 h; (a) undoped ($x = 0, y = 0$); (b) $x = 0, y = 0.025$; (c) $x = 0.025, y = 0.025$; (d) $x = 0.1, y = 0.025$.

12 mm. The green compacts were sintered in covered alumina crucibles at 1150 °C for 2 h in air.

The relative density of the fired specimen was determined by the Archimedes method. The crystal structure was analyzed using an X-ray diffractometer (XRD, RAD III, Rigaku, Japan), and the surface morphology was observed with a field-emission scanning electron microscope (FE-SEM, JEOL, JSM-65OFF, Japan). Electrical measurements were carried out after screen-printing Ag paste onto both sides of the disk-shaped specimen and subsequent firing at 700 °C for 30 min. The polarization–electric field (P–E) and EFIS hysteresis loops were measured in silicon oil using a modified Sawyer–Tower circuit and a linear variable differential transducer, respectively.

3. Results

The microstructures of specimens were observed after polishing and subsequent thermal etching and are shown in Fig. 1. Undoped BNKT, as seen in Fig. 1(a), reveals a dense microstructure with several pores, whose average grain size was found to be 0.82 μm. When up to 2.5 mol% Ti was substituted with Ta, as shown in Fig. 1(b), the average grain size was slightly decreased to 0.78 μm. Further Li doping on A-sites considerably increased the average grain size as clearly seen in Fig. 1(c) and (d). The average grain size of the 10 mol% Li-substituted specimen ($x = 0.1$, $y = 0.025$) was characterized as 1.2 μm. It was also reported that Li substitution into the A-site in BNT-based ceramics not only enhances the grain growth [22–24], but lowers the sintering temperature [25].

Fig. 2 displays X-ray diffraction patterns for sintered specimens. Undoped BNKT ($x = 0$, $y = 0$) revealed peak splittings at around 40° of {1 1 1} reflections and 46° of {2 0 0} reflections, which indicated the coexistence of rhombohedral and

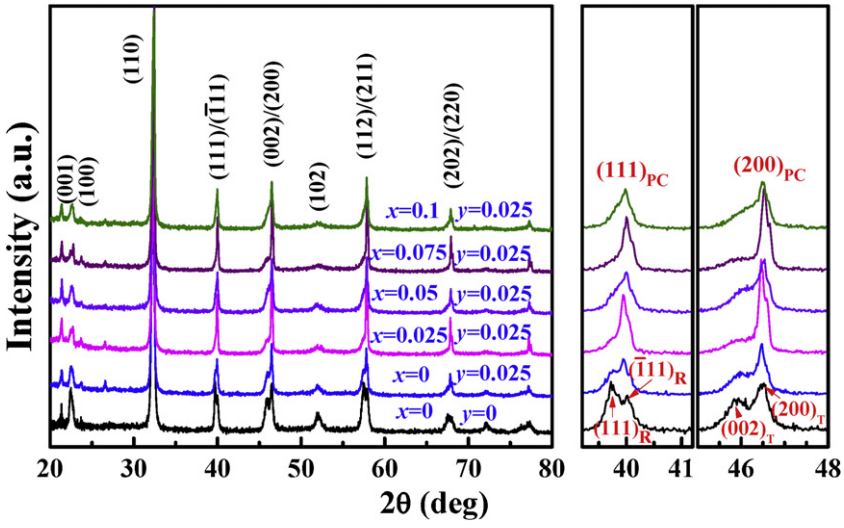

Fig. 2. X-ray diffraction patterns of $(Bi_{0.5}Na_{0.41-x}K_{0.09}Li_x)(Ti_{1-y}Ta_y)O_3$ ceramics at different doping concentrations of Li (x) and Ta (y).

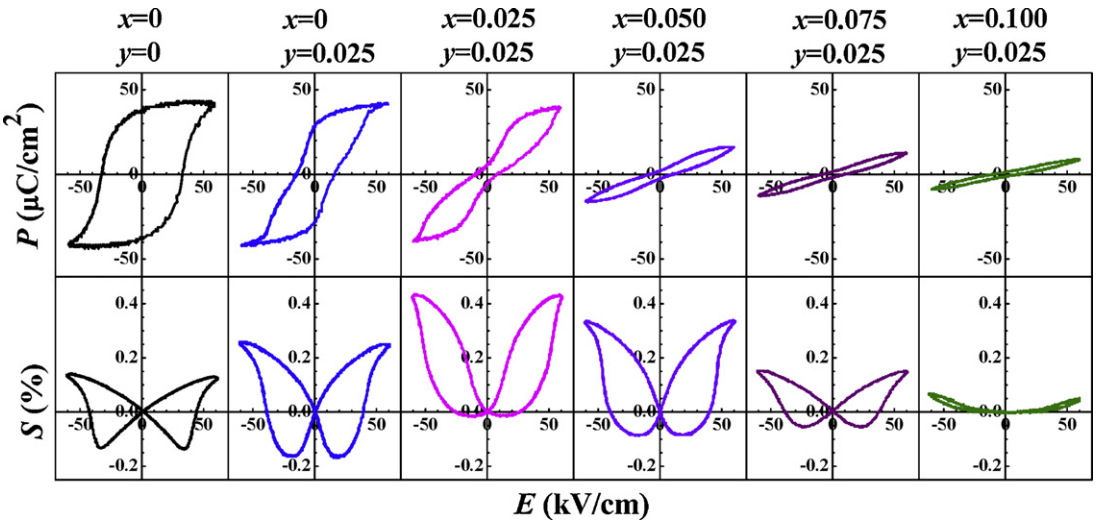

Fig. 3. Effects of Li and Ta doping on the ferroelectric and field-induced strain properties of $Bi_{1/2}(Na_{0.82-x}Li_xK_{0.18})_{1/2}(Ti_{0.975}Ta_{0.025})O_3$ ceramics; (a) *P*–*E* and (b) bipolar *S*–*E* hysteresis loops.

tetragonal phases, consistent with previous studies on BNT–BKT solid solutions [11–15]. The sample at $x = 0$ and $y = 0.025$ that was further substituted with 0.025 mol Ta on B-sites also indicated the coexistence of both ferroelectric phases. As Li was further substituted on A-sites in the range of $x = 0$–0.1, both anisotropic ferroelectric phases transformed into an isotropic pseudocubic phase, which was evidenced by merging of $(1\,1\,1)/(\bar{1}\,1\,1)$ and $(0\,0\,2)/(2\,0\,0)$ into $(1\,1\,1)$ and $(2\,0\,0)$, respectively. Such a transition is also observed in Nb- or Ta-substituted BNKT (82/18) ceramics [20,21], whereas the present result is interesting because Li is an A-site substituent.

The effects of Li and Ta doping on the field-induced polarization (*P*–*E*) and strain (*S*–*E*) hysteresis loops of BNKT ceramics are shown in Fig. 3. In case of unmodified BNKT ($x = 0$ and $y = 0$), typical ferroelectric *P*–*E* and *S*–*E* loops that are characterized by a distinctive squareness in the *P*–*E* loop as well as a butterfly-shaped *S*–*E* curve are observed. In case of 0.025 mol Ta-doped BNKT ($x = 0$ and $y = 0.025$), the specimen reveals a pinched *P*–*E* loop, which is often observed in other modified BNT ceramics [16,17,22,23]. As Li is further doped on A-sites, the *P*–*E* loop becomes close to that of a paraelectric that is distinct as a linear *P*–*E* curve with little remnant polarization P_r, meaning that Li doping promotes a FE–NP phase transition, consistent with the XRD results shown in Fig. 2.

When examining the *S*–*E* loop of 0.025 mol Ta-doped BNKT ($x = 0$ and $y = 0.025$) in Fig. 3, negative strains at E_c and $-E_c$ are observed, which suggests the existence of polar domains that cause a negative strain when domain orientation is reversed. When both Ta and Li concentrations were 0.025 mol ($x = y = 0.025$), the negative strain almost vanishes, implying that there is little ferroelectric domain in the specimens [17]. Further increasing the Li doping level *x* to 0.1 resulted in a parabolic *S*–*E* loop with a markedly decreased strain.

Unipolar field-induced strain is more important in a practical sense because most electromechanical actuators are operated in a unipolar mode. Fig. 4 represents unipolar *S*–*E* loops and S_{max}/E_{max} values of Li- and Ta-doped BNKT ceramics. Undoped BNKT shows an S_{max}/E_{max} value of 230 pm/V, while 0.025 mol Ta doping increases the S_{max}/E_{max} to 432 pm/V. Simultaneous A-site doping with 0.025 mol Li ($x = y = 0.025$) leads to an S_{max}/E_{max} of 727 pm/V, comparable to high end values of soft PZT ceramics [2]. Further Li doping gradually reduces the d^*_{33} to 87 pm/V at $x = 0.1$ as the trend is almost equal to the maximum strain in the bipolar *S*–*E* loops in Fig. 3.

4. Discussion

As seen in previous reports on Nb- or Ta-doped BNKT ceramics [20,21], this study found that Li- and Ta-modified BNKT showed a FE–NP phase transition as the Li content increased. Furthermore, a large strain was induced just after the phase transition. The large strain in Bi perovskites is believed to be associated with the electric field-induced phase transition from a nonpolar pseudocubic or low anisotropy phase to a more asymmetric phase. This transition was recently clarified by synchrotron X-rays [26,27], neutron

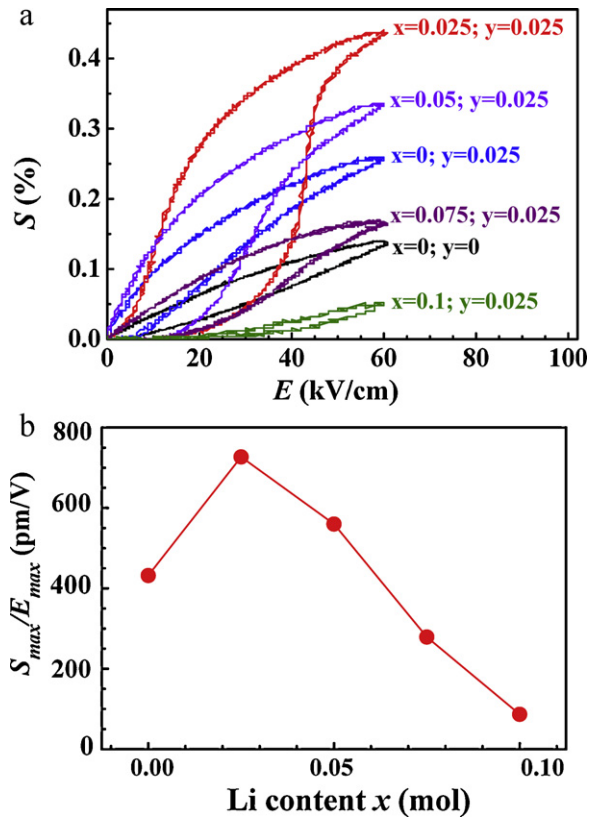

Fig. 4. Effects of Li and Ta doping on (a) unipolar *S*–*E* loop and (b) normalized strain S_{max}/E_{max} of $Bi_{1/2}(Na_{0.82-x}Li_xK_{0.18})_{1/2}(Ti_{0.975}Ta_{0.025})O_3$ ceramics.

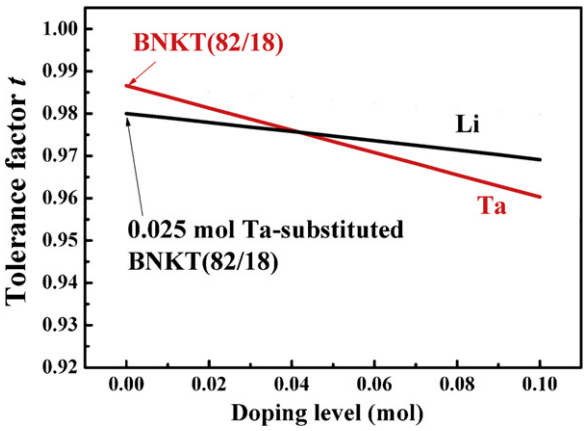

Fig. 5. The tolerance factor of BNKT as a function of Ta and Li doping concentrations.

diffraction [28], transmission electron microscopy [29], and conventional X-ray diffraction [30–34] studies under electric fields. Although nonpolar Bi-perovskites far from the FE–NP phase boundary were recently found to exhibit thermally stable electrostrictive coefficients [35,36], an understanding of the nature of nonpolar or weak polar state near the phase boundary is still lacking.

According to other recent studies on Li-doped BNT-based ceramics [22–25], Li doping on A-sites reduced both P_r and E_c even though their electric field-induced strain behaviors were not examined. The driving force for the FE–NP phase transition in Bi-perovskites, which is one of key aspects in understanding the large strain in these materials, should be considered. A comprehensive analysis of the present results combined with our recent works on BNKT doped with Zr, Hf, Nb, and Ta [18–21] suggests that the FE–NP phase transition occurs when there is a decrease in the Goldschmidt's tolerance factor (t) [37], which is often quoted to explain the stability of the ABO_3 perovskite structure and is given by the following equation;

$$t = \frac{r_A + r_O}{\sqrt{2}(r_B + r_O)} \quad (1)$$

where r_A, r_B, and r_O are the ionic radii of A- and, B-site cations and oxygen, respectively. It was reported that a perovskite crystal structure is stable when t is in the range of 0.85–1.09 [38].

Based upon a Shannon's report [39] on ionic radii for Bi^{3+} (0.117 nm), Na^+ (0.136 nm), K^+ (0.164 nm), Li^+ (0.092), Ti^{4+} (0.0605 nm), Ta^{5+} (0.064 nm), and O^{2-} (0.14 nm), the t of Li- and Ta-doped BNKT was calculated as a function of doping level as displayed in Fig. 5. In case of aliovalent Ta^{5+} doping on Ti^{4+}, the formation of A-site vacancies that are induced to maintain charge valance in the lattice was taken into account for calculating t. It can be seen in Fig. 5 that both Li- and Ta-doping result in reductions in t. This is mathematically related with either larger ion doping on B-sites or smaller ion doping on A-sites. In the present study, Ta^{5+} is larger than Ti^{4+} and further induces an A-site vacancy per two Ta^{5+} ions, which also leads to a decrease in effective size of A-site ions. On the other hand, Li^+ is smaller than the average ionic size calculated on the basis of compositional fractions of A-site cations. Interestingly, by analyzing a wide range of reports on BNT-based ceramics, Lee et al. [40] found that both the small signal piezoelectric constant d_{33} and piezoelectric coupling coefficient k_p in Bi-perovskite piezoelectric ceramics are enhanced as t increases. Consistent with published results, the present study also shows that the ferroelectricity (P_r and E_c) decreases with Li and Ta doping as seen in Fig. 3 to cause reductions in t and lattice anisotropy, resulting in a nonpolar pseudocubic phase at higher Li levels.

Additional evidence for the intimate relationship between t and the FE–NP phase transition is that the slope in Fig. 5 is closely related to the composition span of the FE–NP phase transition region. Fig. 5 illustrates that the FE–NP transition by Li doping would occur more slowly as a function of doping level compared to that with Ta doping. Indeed Li doping in this work results in a slower FE–NP transition as a function of composition compared to that with Ta doping. In the case of Ta-doped BNKT, the transition occurred much faster in terms of doping level, similar to the results of a previous report [21], while Li-doped BNKT exhibited a transition spanning over 0–0.1 mol, as seen in Fig. 3. This fact is of practical importance because a higher process tolerance regarding composition can be established. The normalized strain (S_{max}/E_{max}) of the Li-doped BNKT shown in Fig. 4 is less sensitive to doping level in comparison with that of Ta-doped BNKT [21].

It should be noted that the normalized strain S_{max}/E_{max} of 727 pm/V obtained in this work is higher than those recently reported on other B-sited modified BNKT ceramics [18–21] that were in the range of 475–641 pm/V. One possible explanation might be that Li- and Ta-doped BNKT is more flexible under electric fields because lattice strains by A- and B-site dopants as well as A-site vacancies complexly contribute to the weakening of $[BO_6]$ distortion in the Bi-perovskite structure even though an exact understanding requires further studies.

5. Conclusions

The effects of co-doping with Ta- and Li-ions on the microstructure, crystal structure, ferroelectric, and EFIS properties of BNKT ceramics were investigated. It was found that Li doping on A-sites also leads to a FE–NP phase transition, as found in other previous reports on B-site doping, resulting in a large strain near the phase boundary. Such a phase transition is strongly believed to be induced by a decrease in the tolerance factor of ABO_3 perovskite structure, which is also evidenced by the fact that Li doping shows a more diffuse FE–NP phase transition than Ta doping.

Acknowledgements

This work was financially supported by the National Research Foundation (NRF), Republic of Korea, under contract no. 2010001-4113 and was partially supported by the Ministry of Education, Science and Technology (MEST) of Korea and the NRF through the Human Resource Training Project for Regional Innovation.

References

[1] T. Takenaka, H. Nagata, J. Eur. Ceram. Soc. 25 (2005) 2693–2700.
[2] T.R. Shrout, S.T. Zhang, J. Electroceram. 19 (2007) 111–124.
[3] J. Rödel, W. Jo, K.T.P. Seifert, E.M. Anton, T. Granzow, J. Am. Ceram. Soc. 92 (2009) 1153–1177.
[4] T. Takenaka, H. Nagata, Y. Hiruma, IEEE Trans. Ultrason. Ferroelectr. Freq. Control 56 (2009) 1595–1612.
[5] G.A. Smolensky, V.A. Isupov, A.I. Agranovskaya, N.N. Krainik, Sov. Phys. Solid State 2 (1961) 2651–2654.
[6] T. Takennaka, K. Maruyama, K. Sakata, Jpn. J. Appl. Phys. 30 (9B) (1991) 2230–2236.
[7] A. Herabut, A. Safari, J. Am. Ceram. Soc. 80 (1997) 2954–2958.
[8] C.E. Peng, J.F. Li, W. Gong, Mater. Lett. 59 (2005) 1576–1580.
[9] X. Chen, X. Gong, T. Li, Y. He, P. Liu, J. Alloys Compd. 507 (2010) 535–541.
[10] H. Ni, L. Luo, W. Li, Y. Zhu, H. Luo, J. Alloys Compd. 509 (2011) 3958–3962.
[11] A. Sasaki, T. Chiba, Y. Mamiya, E. Otsuki, Jpn. J. Appl. Phys. 38 (1999) 5564–5567.
[12] H. Ishii, H. Nagata, T. Takenaka, Jpn. J. Appl. Phys. 40 (2001) 5660–5663.
[13] K. Yoshii, Y. Hiruma, H. Nagata, T. Takenaka, Jpn. J. Appl. Phys. 45 (2006) 4493–4496.
[14] Y. Zhang, R. Chu, Z. Xu, J. Hao, Q. Chen, F. Peng, W. Li, G. Li, Q. Yin, J. Alloys Compd. 502 (2010) 341–345.
[15] X. Chen, Y. Liao, H. Wang, L. Mao, D. Xiao, J. Zhu, Q. Chen, J. Alloys Compd. 493 (2010) 368–371.
[16] S.T. Zhang, A.B. Kounga, E. Aulbach, J. Rödel, Appl. Phys. Lett. 91 (2007) 112906.
[17] S.T. Zhang, A.B. Kounga, E. Aulbach, T. Granzow, W. Jo, H.J. Kleebe, J. Rödel, J. Appl. Phys. 103 (2008) 034107.
[18] A. Hussain, C.W. Ahn, A. Ullah, J.S. Lee, I.W. Kim, Jpn. J. Appl. Phys. 49 (2010) 041504.

[19] A. Hussain, C.W. Ahn, J.S. Lee, A. Ullah, I.W. Kim, Sens. Actuator A 158 (2010) 84–89.
[20] K.N. Pham, A. Hussain, C.W. Ahn, I.W. Kim, S.J. Jeong, J.S. Lee, Mater. Lett. 64 (2010) 2219–2222.
[21] N.B. Do, H.B. Lee, C.H. Yoon, J.K. Kang, J.S. Lee, I.W. Kim, Trans. Electr. Electron. Mater. 12 (2011) 64–67.
[22] X.Y. Wang, C.L. Wang, M.L. Zhao, J.F. Wang, K. Yang, J.C. Li, Mater. Lett. 61 (2007) 3847–3850.
[23] Y.J. Dai, S. Zhang, T.R. Shrout, X.W. Zhang, J. Am. Ceram. Soc. 93 (2010) 1108–1113.
[24] N. Lei, M. Zhu, P. Yang, L. Wang, L. Wang, Y. Hou, H. Yan, J. Appl. Phys. 109 (2011) 054102.
[25] D. Lin, K.W. Kwok, Curr. Appl. Phys. 10 (2010) 1196–1202.
[26] K.G. Webber, Y. Zhang, W. Jo, J.E. Daniels, J. Rödel, J. Appl. Phys. 108 (2010) 014101.
[27] D. Lin, D. Xiao, J. Zhu, P. Yu, Appl. Phys. Lett. 88 (2006) 062901.
[28] J.E. Daniels, W. Jo, J. Rödel, J.L. Jones, Appl. Phys. Lett. 95 (2009) 032904.
[29] J.E. Daniels, W. Jo, J. Rödel, V. Honkimäki, J.L. Jones, Acta Mater. 58 (2010) 2103–2111.
[30] L.A. Schmitt, M. Hinterstein, H.J. Kleebe, H. Fuess, J. Appl. Cryst. 43 (2010) 805–810.
[31] J. Kling, X. Tan, W. Jo, H.J. Kleebe, H. Fuess, J. Rödel, X. Tan, J. Am. Ceram. Soc. 93 (2010) 2452–2455.
[32] W. Ge, H. Cao, J. Li, D. Viehland, Q. Zhang, H. Luo, Appl. Phys. Lett. 95 (2009) 162903.
[33] M. Hinterstein, M. Knapp, M. Hölzel, W. Jo, A. Cervellino, H. Ehrenberg, H. Fuess, J. Appl. Crystallogr. 43 (2010) 1314–1321.
[34] G. Picht, J. Töpfer, E. Hennig, J. Eur. Ceram. Soc. 30 (2010) 3445–4353.
[35] K.T.P. Seifert, W. Jo, J. Rödel, J. Am. Ceram. Soc. 93 (2010) 1392–1396.
[36] V.D.N. Tran, H.S. Han, C.H. Yoon, J.S. Lee, W. Jo, J. Rödel, Mater. Lett. 65 (2011) 2607–2609.
[37] V.M. Goldschmidt, Skrifer Norske Videnskaps–Akad. Oslo, I. Mat.–Nat. Kl. 8 (1926).
[38] O. Muller, R. Roy, The Major Ternary Structural Families, Springer, New York, 1974, p. 221.
[39] R.D. Shannon, Acta Crystallogr. A, 32 75 (1976) 1–767.
[40] W.C. Lee, C.Y. Huang, L.K. Tsao, Y.C. Wu, J. Eur. Ceram. Soc. 29 (2009) 1443–1448.